A Novel Approach to Estimate Depth and Reflectance Maps in Participating Media

László Neumann[1], Rafael Garcia[1], Jordi Ferrer[1], and Attila Neumann[2]

Institute of Informatics and Applications
University of Girona, Spain

Abstract. A new technique to simultaneously determining the three-dimensional geometry and reflectance map of a scene in underwater imaging will be presented. Underwater light is affected by an exponential wavelength-dependent absorption effect. These special conditions make image and video processing a difficult task. In this paper it is shown how to use this disturbing absorption effect to find a new way to accurately estimate the scene depth-map and multispectral reflectivities. The process requires the acquisition of a multispectral image of the underwater scenario with appropriate camera and light source arrangement. In addition, the method also allows the computation of the normal vectors of every point of the reconstructed scene. In contrast to usual approaches, our algorithm does not require any information of the neighborhood to compute the surface normal at a given point. Thereby, this estimation is stable at depth-discontinuities.
The algorithm has been tested on several synthetic images for different noise levels. The promising results show that the technique provides accurate and stable results.

1 Introduction

Depth-map reconstruction at pixel level is an important problem in computer vision [11]. Many techniques have appeared in the past to recover three-dimensional scene structure from two-dimensional images. A possible classification of these techniques broadly divides them into passive and active methodologies. The most popular passive techniques are stereo [2] or "structure from motion", which use multiple views to resolve structure ambiguities inherent in a single image. The main bottleneck of these methods is solving the correspondence problem [13], which is even more difficult in the case of underwater imaging. Another widely-used passive technique is "depth from defocus" [7], where the relationship between focused and defocused images is computed. As in the case of the previous techniques, depth from defocus requires scenes with enough texture frequency. With respect to the second category, among active techniques, light stripe methods appear as the most popular range sensing techniques. However, to achieve depth-maps with sufficient spatial resolution, a large number of closely spaced stripes has to be used. This implies projecting one stripe at a time, and acquiring a sequence of images to be able to associate a unique stripe with a given pixel. In this case, a large number of images is necessary to obtain dense reconstructions. Evolution of this technique gave rise to assignation of gray-codes to the stripes, reducing the number of required images [12], or the use of color-coded stripe patterns [1], which reduce the number of required images to 1. The inherent weakness of this approach is the difficulty in segmentation of the stripes in a real scenario which reflects differently many wavelengths of light.

Recovering dense depth-maps is even more difficult if we consider an underwater scene. A major obstacle to processing images of the ocean floor is related to the special transmission properties of the light in the underwater medium [5]. Light suffers two different processes in the aquatic environment [3]: (*i*) absorption, where light "disappears" from the image-forming process, and (*ii*) scattering, unwanted multiple inter-reflection in the medium. These transmission properties of the medium causes blurring of image features and limited visual range [4, 6].

In this paper we propose a novel method for estimating the depth-map of an underwater scene by exploiting the attenuation coefficients of the water. At the same time, the mathematical derivation will allow also to recover the reflectance properties of the scene for some wavelengths (typically in the bluish range). A closed form solution to the estimation of a dense depth-map is provided.

2 Camera and lighting arrangement

In underwater imaging, and especially in deep ocean applications, the "longest" visual range is obtained by means of using only a limited interval of the spectrum in the bluish range [5]. Unfortunately, also the use of the bluish range is limited to a few tens of meters. We suggest the use of standard flash lamps and narrow-band filters. Despite the fact that this seems an energy-consuming approach, it

is better than the efficiency of laser techniques. The proposed method does not need time consuming scanning, as required by laser, but taking single shots with 2 or 3 lamps a large area can be processed.

Let us consider 3 spectral channels to illustrate our new method for depth-map reconstruction. These channels are not pure spectral colors but tight spectral windows according to band-pass filters of 5-20 nm. In a small spectral window we can assume a homogenous, nearly constant behavior of the most important optical parameters, like scattering and absorption.

For simplicity, let us call the 3 channels r, g and b, although they can represent *e.g.* 460-480, 440-460, 420-440 nm, three bluish intervals in deep ocean water. Consider we have several point light sources. In practice we can use flashes with lenses and optical filters to create a pinhole-like light source. The narrow-band filters could be either (*i*) built in a multispectral camera, (*ii*) placed in front the lens of a standard grayscale camera, or (*iii*) applied directly to the light sources. Let k be the index of light sources ($\mathbf{L}_k$). Two lamps are required with known spatial energy distribution, and known extrinsic (position and orientation) parameters. The use of a higher number of lights provides redundancy, thus, increasing accuracy.

Prior to the experiments, both the intrinsic and extrinsic parameters of the camera have to be modeled through calibration, together with the geometry of the light sources with respect to the camera. In addition, the absorption factors of the 3 channels (a_R, a_G, a_B) have to be obtained also through calibration. Let us assume that the absorption factors do not change in the field of view and that the reflectance models, *i.e.*, the Bidirectional Reflectance Distribution Functions (BRDFs), have the following properties: the ratio of reflected rgb radiance values is practically constant for the used light and view directions. That is true for a diffuse material, but also for a wider class of BRDFs where the shape of the distribution is similar at every wavelength, differing only by a linear multiplicative factor. Replacing the 3 "pseudo" rgb channels with "real" rgb colors a pseudo color image can be created, typically with low-saturated colors. Namely, the differences of 3 neighboring bluish narrow-bands in the reflectance curve are small. In order to obtain enhanced colorful images with increased contrast [9] or [10] can be applied.

3 Computing depth and reflectance

3.1 The basic equations

In order to determine the depth-map it is enough to use 2 of the above mentioned "pseudo" rgb channels to derive the equations. Let us assume we work only with 2 wavelengths. For simplicity let us call the used λ_1 and λ_2 wavelengths r and g, independently of its real value.

We will demonstrate the method for diffuse materials. In this case the BRDF is a simple constant value [8]. Strictly, the BRDFs are:

$$BRDF_r = \frac{r}{\pi}[sr^{-1}], \qquad BRDF_g = \frac{g}{\pi}[sr^{-1}] \tag{1}$$

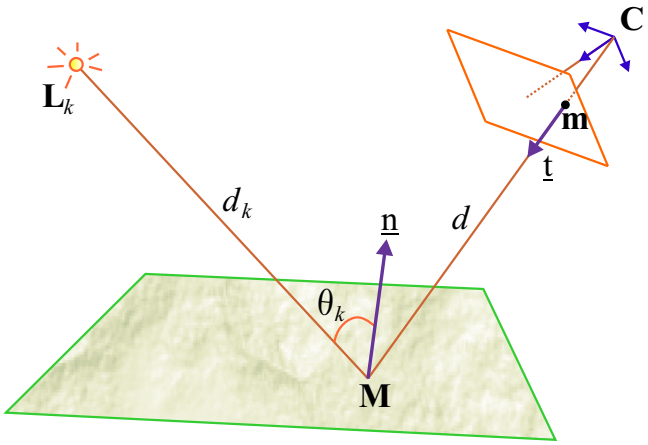

Fig. 1. Projection of a 3D world point **M** onto the image plane (**m**); d defines the unknown distance from scene point **M** the focal point **C** of the camera, while d_k is the distance from lamp k to **M**, and Θ_k defines the angle between the incident light from light source k and the surface normal $\underline{\mathbf{n}}$ at point **M**

where r and g are the "reflectivity" values in the interval $[0, 1]$.

Consider a scene point **M**, which is projected into the image plane at coordinates $\mathbf{m} = (x_i, y_i)$ (see Fig. 1). For a given lamp k, every pixel **m** of the image defines the following equations:

$$R_k = \frac{1}{4\pi^2} \cdot r_k \cdot \cos\Theta_k \cdot P_{Rk} \cdot d_k^{-2} \cdot e^{(-a_R \cdot d)} \cdot e^{(-a_R \cdot d_k)} \tag{2}$$

$$G_k = \frac{1}{4\pi^2} \cdot g_k \cdot \cos\Theta_k \cdot P_{Gk} \cdot d_k^{-2} \cdot e^{(-a_G \cdot d)} \cdot e^{(-a_G \cdot d_k)} \tag{3}$$

where d is the unknown distance from scene point **M** to the focal point **C** of the camera; d_k is the distance from lamp k to **M**; (r_k, g_k) define the reflectivity, or more precisely the reflected radiance of scene point **M** for the lamp $\mathbf{L}_k$ and view point geometry, according to eq. (1); Θ_k is the light incident angle; (P_{Rk}, P_{Gk}) defines the power of lamp k at wavelengths r_k and g_k; and (a_R, a_G) are the absorption factors. To illustrate their effect, consider an absorption parameter $a = 0.2$, then the radiance will be $e^{-0.2 \cdot 1} = 0.8187$ times smaller after 1 meter. Finally, (R_k, G_k) are the incoming radiance values $[Wm^{-2}sr^{-1}]$, which can be computed after appropriate calibration from the pixel signal of the camera and the exposure time. It should be noted that we have used in eqs. (2–3) the multiplicative constant $\frac{1}{4\pi^2}$ coming from the factor $\frac{1}{\pi}$ in eq. (1) and from the factor $\frac{1}{4\pi}$ describing the irradiance at point **M**. Namely, the mentioned irradiance value is $P_k/(4\pi d_k^2)$.

The intrinsic parameters of the camera can be modeled through calibration. Thereby, view direction is known for every pixel. We aim to determine the

camera-scene distance at pixel resolution (d), to obtain a dense depth-map of the scene.

The unknowns in eqs. (2–3) are d, d_k, r_k, g_k and Θ_k. Therefore, for every pixel, 5 unknowns and 2 equations are obtained for every lamp k. Let us consider the minimal required number of lamps, i.e. 2, and assume that both light sources reach point $\mathbf{M}$. An additional constraint arises from the dependence of d_k as a function of d, according to the spatial geometry of the camera-light sources. In order to solve for the unknowns we use logarithmic scales. The difference of logarithm of eq. (2) and eq. (3) is the logarithm of the ratio of eq. (2) and eq. (3). First, we compute the difference between eqs. (2) and (3) for $k = 1$, as shown in eq. (4). Then, the difference between eqs. (3) and (2) for the second light source ($k = 2$) (see eq. (5)).

$$\ln R_1 - \ln G_1 = \ln r - \ln g + \ln P_{R1} - \ln P_{G1} + d(a_G - a_R) + d_1(a_G - a_R) \quad (4)$$

$$\ln G_2 - \ln R_2 = \ln g - \ln r + \ln P_{G2} - \ln P_{R2} + d(a_R - a_G) + d_2(a_R - a_G) \quad (5)$$

Fortunately, proceeding in this way Θ_k disappears from the equations. The sum of eqs. (4-5) results in the expression of eq. (6).

$$\rho + P = d_1(a_G - a_R) + d_2(a_R - a_G) \quad (6)$$

where ρ is a value which depends on the ratio of R_k and G_k; and the constant P depends on the power of the light sources. To ensure a solvable eq. (6) we have to select wavelengths where $a_R \neq a_G$.

$$\rho = \ln R_1 - \ln R_2 - \ln G_1 + \ln G_2 \quad (7)$$

$$P = -\ln P_{R1} + \ln P_{G1} - \ln P_{G2} + \ln P_{R2}, \quad (8)$$

thus, eqs. (7) and (8) can be expressed as:

$$\rho = \ln\left(\frac{R_1 \cdot G_2}{R_2 \cdot G_1}\right) \qquad P = \ln\left(\frac{P_{R2} \cdot P_{G1}}{P_{R1} \cdot P_{G2}}\right) \quad (9)$$

With this approach, the terms containing r or g eliminate each other. Eq. (6) is a non-linear function of the unknowns d_1 and d_2, which can be solved by iteration. We can write eq. (6) as:

$$\rho + P = (a_G - a_R)(d_1 - d_2) \quad (10)$$

Writing d_1 and d_2 as a function of the depth d of image point $\mathbf{m}$ (see Fig. 1):

$$d_k(d) = \|\mathbf{M} - \mathbf{L}_k\| \quad (11)$$

Since $\mathbf{M} = \mathbf{C} + d \cdot \underline{\mathbf{t}}$, being $\mathbf{M}$ the 3D coordinates of the imaged scene point, $\mathbf{C}$ the 3D position of the camera focal point and $\underline{\mathbf{t}}$ the unit vector[1] of the viewing

[1] In order to provide a clearer view to the reader, unit vectors are written in underline form ($\underline{\_}$)

direction, which can be computed from the intrinsic parameters of the camera. Therefore, eq. (11) can be written as:

$$d_k(d) = \|\mathbf{C} + d \cdot \underline{\mathbf{t}} - \mathbf{L}_k\| \tag{12}$$

$$d_k(d) = \left[\sum_j (C_j + d \cdot t_j - L_{kj})^2\right]^{\frac{1}{2}} \tag{13}$$

with j being the x, y and z coordinates.

3.2 Closed form solution

Expanding eq. (**??**), the distance d_k from every pixel to lamp k can be expressed as a function of d in the form $d_k(d) = \sqrt{d^2 + b_k \cdot d + c_k}$, where only d is unknown and b_k and c_k are constants. Retaking eq. (10), we can write:

$$\frac{\rho + P}{a_R - a_G} = d_1 - d_2 \tag{14}$$

Now, we can define the constant $B = d_1 - d_2$ and considering d_k as expressed above, for the two lamps, d_1 and d_2 eq. (15) is obtained:

$$B = \sqrt{d^2 + b_1 \cdot d + c_1} - \sqrt{d^2 + b_2 \cdot d + c_2} \tag{15}$$

Squaring and simplifying eq. (15), two possible solutions for d can be obtained

$$d = \frac{\lambda \pm 2 \cdot \sqrt{\psi}}{\tau} \tag{16}$$

with

$$\begin{aligned}
\lambda &= -B^2 \cdot (b_1 + b_2) + b_2 \cdot (c_2 - c_1) + b_1 \cdot (c_1 - c_2) \\
\psi &= B^2 \cdot ((c_1 \cdot (-2 \cdot c_2 + c_1 + b_2 \cdot (b_2 - b_1))) \\
&\quad + (c_2 \cdot (c_2 + b_1^2)) \\
&\quad + (b_1 \cdot b_2 \cdot (B^2 - c_2)) \\
&\quad + (B^2 \cdot (B^2 - 2 \cdot (c_1 + c_2)))) \\
\tau &= 4 \cdot B^2 + 2 \cdot b_2 \cdot b_1 - b_2^2 - b_1^2
\end{aligned}$$

The correct root of eq. (16) is selected through the following strategy. Consider 3 light sources and 3 wavelengths in a real scenario. Nine noisy d values for every pixel will be obtained according to eq. (16). Then, d can be estimated as the median of the 9 noisy solutions. However, since eq. (16) comes from a quadratic equation, it provides 2 different solutions for every selected pair of lamps and wavelengths. In some cases, one of the non-real solutions can be rejected easily knowing the geometrical arrangement, obtaining a unique solution. Unfortunately, there are problematic cases where both solutions satisfy all the

equations (6) to (16). In this situation, the selection of the correct solution is a hard problem, which cannot be solved through a simple geometrical analysis. In this case, we ignore both of these two solutions, obtaining less than 9 d values. Finally, the median of the unique solutions will be accepted as the estimated depth value. If none of the 9 pairs gives any unique solution for d, the depth map of this point will remain unknown. Fortunately, these cases are rather unfrequent.

3.3 Particular camera-light source arrangement

In this section we develop the equations of a special case in the arrangement of the geometry of the system. If one of the light sources is located at the focal point of the camera (e.g. through a *beamsplitter* as in the case of vision the systems used in industry), one of the square roots in equation (15) can be eliminated. Then, a simpler equation containing only one root can be obtained. Consider the case where $\mathbf{L}_1$ is located at the focal point ($d_1 = d$). The following equation is obtained:

$$B = d - \sqrt{d^2 + b_2 \cdot d + c_2}$$
$$d = \frac{-c_2 + B^2}{b_2 + 2 \cdot B}$$

or, if the lamp $\mathbf{L}_2$ is located at the focal point ($d_2 = d$):

$$B = d + \sqrt{d^2 + b_1 \cdot d + c_1}$$
$$d = \frac{-c_1 + B^2}{-b_1 + 2 \cdot B}$$

3.4 Removing the absorption effect

Having an image with absorption for every lamp, and knowing d and d_k values for every pixel, we can remove the unwanted absorption effect by dividing the pixel radiances R_k and G_k of eqs. (2–3) by $e^{-a_R(d+d_k)}$ and $e^{-a_G(d+d_k)}$, respectively. Proceeding in this way, a different image is obtained for every lamp. All these images can be merged into a single image by a linear combination of these absorption-less images.

The final step is to determine r and g reflectivities, knowing d and d_k values. Writing eqs. (2–3) for lamps $k = 1$ and $k = 2$, we obtain 4 equations and the 4 unknowns: r, g, $cos\Theta_1$ and $cos\Theta_2$. After logarithmic transformation, the appropriate linear equation system can be solved.

Having more than 2 lamps, we can build –for every selected pair of lamps– eqs. (2–10). This redundancy increases the accuracy or enables the computation of the surface points which may be in shadow for some of the lamps. Having L active lamps for a given pixel, and using W different wavelengths, we can build a total number of $\binom{L}{2} \cdot \binom{W}{2}$ different equation systems with appropriate power selection in eq. (8).

The median value or RANSAC-like estimation of the reflected radiances for the active lamps provides the desired reflectance values.

4 Estimation of the normal vectors of the surface

The depth-map of the part of the scene acquired by the camera can be calculated using only 2 light sources. If 3 lamps are used, in addition to the depth-map, the surface normal vectors can also be determined for those points of the scene that receive light from the 3 light-sources.

Consider the 3D point $\mathbf{M}$, which belongs to the surface. Knowing the depth-map d at point $\mathbf{M}$, the coordinates of $\mathbf{M}$ can be computed provided that $\mathbf{M} = \mathbf{C} + d \cdot \underline{\mathbf{t}}$ (see fig. 1). Therefore, vector $\mathbf{l}_k$ can be expressed as $\mathbf{l}_k = \mathbf{M} - \mathbf{L}_k$, and $\underline{\mathbf{l}}_k$ is the unit norm version of $\mathbf{l}_k$

$$\underline{\mathbf{l}}_k = \frac{\mathbf{M} - \mathbf{L}_k}{\|\mathbf{M} - \mathbf{L}_k\|}$$

If the unknown surface normal $\mathbf{n}$ at point $\mathbf{M}$ were a unit vector ($\underline{\mathbf{n}}$), then the cosine factor in eq. (3) would be simply the scalar product of the two unit vectors $\underline{\mathbf{l}}_k$ and $\underline{\mathbf{n}}$:

$$\underline{\mathbf{l}}_k \cdot \underline{\mathbf{n}} = \cos\theta_k \qquad (k = 1, 2, 3) \tag{17}$$

The k indices in eq. (17) refer to the 3 selected lamps. The positivity condition $\underline{\mathbf{l}}_k \cdot \underline{\mathbf{n}} > 0$ holds, because the two normal vectors point towards the same half-space and neither lighting nor the visibility are perfectly tangential. The length of $\underline{n}$ is unknown, thus the $\cos\theta_k$ values are also unknown. Fortunately, knowing the depth-map, the value of the product $r_k \cdot \cos\theta_k$ (or for other wavelength) can be computed from eqs. (2) or (3). For now let us concentrate on a single wavelength and the 3 selected lamps. They determine a linear equation system of 3 unknowns, namely of the components of the non-normalized surface normal vector $\mathbf{n}$.

$$\begin{aligned} \underline{\mathbf{l}}_1 \cdot \mathbf{n} &= r_1 \cdot \cos\theta_1 \\ \underline{\mathbf{l}}_2 \cdot \mathbf{n} &= r_2 \cdot \cos\theta_2 \\ \underline{\mathbf{l}}_3 \cdot \mathbf{n} &= r_3 \cdot \cos\theta_3 \end{aligned} \tag{18}$$

where the product terms $(r_k \cdot \cos\theta_k)$ are known, and $\underline{\mathbf{l}}_k$ can be computed from the estimated d. The remaining unknowns are r_k and the normal vector $\mathbf{n}$, provided that $\cos\theta_k = \underline{\mathbf{l}}_k \cdot \underline{\mathbf{n}}$ if $\|\underline{\mathbf{l}}_k\| = \|\underline{\mathbf{n}}\| = 1$.

Solving the linear system (18) the elements n_x, n_y and n_z of the non-normalized vector $\mathbf{n}$ are obtained. Then, knowing $\mathbf{n}$, his normalized form $\underline{\mathbf{n}}$ can be computed, and we will obtain from eq. (17) the $\cos\theta_k$ values. Finally, we determine, having all of other numbers, from eq. (18) the reflectance or BRDF values r_1 , r_2 and r_3 values, which depend on light and viewpoint geometry, can be obtained. Similarly, the appropriate reflectance values can be computed for the other wavelengths.

It is important to note that our proposal to compute the surface normals is not based not on a finite difference like in local estimation methods, where integration is used at neighbouring pixel-depths [14]. This new approach allows the direct computation of the surface normals, independently of the normal vectors in the neighbourhood. Thereby, this estimation is stable at depth-discontinuities. Furthermore, the reflectance value of the surface is obtained for the selected wavelengths as a "side-effect".

5 Simulation Results

In order to prove the correctness of the proposed approach we have carried out extensive simulations. Consider a scene with the camera facing downwards, simulating the situation of an underwater robot navigating close to the ocean floor. The camera is located at a distance of 8 meters over the seabed. Three light sources have been placed as illustrated in Fig. 2. It can be noted that in this case the light sources are located at relative small incident angles to avoid large shadows induced in the scene.

A real CCD camera has been simulated by rounding the floating point values of the image into 16-bit integer numbers. The simulated camera is the *HiRes IV Plus* from *DTA*, which integrates a *Kodak CCD* (model *KAF-1301LE*), and the noise added to the image corresponds to the specifications of the manufacturer. Fig. 3(a) illustrates a sample synthetic image, which simulates an underwater scene with a typical bluish fast-darkening effect. The absorption parameters have been selected slightly high in this example (around 0.15 for every wavelength), differently from the true deep ocean values, being them about 2 or 3 times smaller according to the data provided in [5] for the deep ocean. The reason of this selection was to study the nature of numerical errors, which in normal situation are significantly less. We can observe in fig. 3(a) how colors are darker and more saturated at the top corners, according to the longest light paths.

The original image has been perturbed by a zero-mean Gaussian noise (according to *DTA*) with $\sigma = 1.3$, and the equations for the depth and reflectance maps have been solved. Taking into consideration 3 light sources and 3 wavelengths, the depth of every pixel is computed according to eq. (16). Fig. 3(b) shows the result of removing the absorption by means of the proposed approach. The colors in this image correspond to the originally selected BRDFs with the shadowing effects.

In order to prove the goodness of the method, noise has been added not only to the image acquired by the camera, but to the parameters that should be calibrated. The absorption parameters of the medium can be calibrated by means of a standard underwater spectrophotometer. We have added noise to the absorption parameters according to the specifications of the *ac-9* device by *WET Labs*. Besides, the extrinsic parameters of the camera (position and orientation of the camera and light sources) have been perturbed with arbitrary noise. Finally, the power of the lamps can be calibrated by means of a spectral lightmeter (e.g. *PR-650 SpectraScan Colorimeter* by *Photo Research*). Again, noise has been

added to the system according to the specifications of the manufacturer. On the other hand, fig. 3 shows the obtained reflectance and 3D reconstruction of the scene, after adding all the noise described above. The obtained depth-map is illustrated in Fig. 5.

As a summary, Table 1 illustrates the performance of the algorithm under different conditions. The first row proves the correctness of the presented method. The average and standard deviation error are presented in the first and second columns and expressed in meters. The last column shows the percentage of the image that has not been reconstructed since the depth-map could not be computed through the algorithm presented in section 3.2. The second and third rows of the table show the results of estimating the depth-map after quantization of the image with 16 bits without noise and with Gaussian noise added to the image, respectively. The next row shows the result of applying the different sources of error to the system, i.e. noise in the extrinsic parameters, estimated power of the lamps and absorption parameters. The worst case when all the possible sources of error occur is illustrated in the last row, where the two previous sources of error (image and calibrated parameters) are applied before reconstructing the scene. Also in this case, the resulting depth-map presents an average depth error of less than 3 cm for a distance of more than 8 meters.

Table 1. Summary of the performance of the algorithm under different conditions

	Average Error	**Std. Error**	**Not Reconstructed**
Continuous	$2.3544 \cdot 10^{-14}$ m	$2.0377 \cdot 10^{-14}$ m	0.0 %
Discrete 16 bits	$6.2043 \cdot 10^{-3}$ m	$6.2027 \cdot 10^{-3}$ m	1.2374 %
D16 - RGB Noise	$1.8673 \cdot 10^{-2}$ m	$1.8418 \cdot 10^{-2}$ m	5.3830 %
D16 - Param. Noise	$2.1764 \cdot 10^{-2}$ m	$1.5635 \cdot 10^{-2}$ m	29.8656 %
D16 - All Noise	$2.8926 \cdot 10^{-2}$ m	$2.2397 \cdot 10^{-2}$ m	34.1474 %

6 Conclusions

Depth-map estimation using structure from motion techniques is susceptible to poor density and limited accuracy in underwater imaging. In addition, it is important in many applications to obtain accurate and dense depth-map and reflectivities of the scene. The theoretical background to recover pixel-dense depth and reflectance maps using a new strategy has been presented. The otherwise undesired absorption of the medium allows the method to work, taking advantage of this unwanted effect. This scene reconstruction is not only valid for diffuse materials (with constant BRDF), but for a wide class of materials, having "non-color-changing" BRDFs. The approach can be applied to any scene in a participating medium, after computation of the system intrinsic and extrinsic

parameters and the absorption coefficients of the medium for the selected wavelengths. Finally, we have proposed a methodology to compute the normal vectors of the surface without the need of neighbouring points information. The algorithm has been tested on several synthetic images for different noise levels. The promising results show that the technique provides accurate and stable results.

References

1. J. Batlle, E. Mouaddib, and J. Salvi. A survey: Recent progress in coded structured light as a technique to solve the correspondence problem. *Pattern Recognition*, 31(7):963–982, 1998.
2. O.D. Faugeras and G. Toscani. The calibration problem for stereo. In *IEEE Conference on Computer Vision and Pattern Recognition*, pages 15–20, 1986.
3. R. Garcia, T. Nicosevici, and X. Cufi. On the way to solve lighting problems in underwater imaging. In *MTS/IEEE OCEANS Conference*, pages 1018–1024, Biloxi, Mississipi, 2002.
4. H.R. Gordon. Absorption and scattering estimates from irradiance measurements: Monte carlo simulations. *Limnology and Oceanography*, 36:769–777, 1991.
5. J.S. Jaffe. The domains of underwater visibility. In *SPIE Ocean Optics VIII*, pages 287–293, 1986.
6. H. Loisel and D. Stramski. Estimation of the inherent optical properties of natural waters from irradiance attenuation coefficient and reflectance in the presence of Raman scattering. *Applied Optics*, 39:3001–3011, 2000.
7. S.K. Nayar, M. Watanabe, and M. Noguchi. Real-time focus range sensor. *PAMI*, 18(12):1186–1198, 1996.
8. L. Neumann and A. Neumann. Radiosity and hybrid methods. *ACM Trans. Graph.*, 14(3):233–265, 1995.
9. E. Pichon, M. Niethammer, and G. Sapiro. Color histogram equalization through mesh deformation. In *ICIP*, volume 2, pages 117–120, 2003.
10. E. Reinhard, M. Ashikhmin, B. Gooch, and P. Shirley. Color transfer between images. *IEEE Comput. Graph. Appl.*, 21(5):34–41, 2001.
11. L. Robert and R. Deriche. Dense depth map reconstruction: A minimization and regularization approach which preserves discontinuities. In *ECCV '96: Proceedings of the 4th European Conference on Computer Vision-Volume I*, pages 439–451. Springer-Verlag, 1996.
12. T. Sato. Multispectral pattern projection range finder. In *SPIE Conference on Three-Dimensional Image Capture and Applications II, vol. 3640*, page 28–37, San Jose, California, 1999.
13. D. Scharstein and R. Szeliski. A taxonomy and evaluation of dense two-frame stereo correspondence algorithms. *IJCV*, 47(1):7–42, 2002.
14. K. Tamal, D. Gang, and L. J. Sun. Normal estimation for point clouds: A comparison study for a voronoi based method. In *Eurographics Symposium on Point-Based Graphics*, New York, 2005.

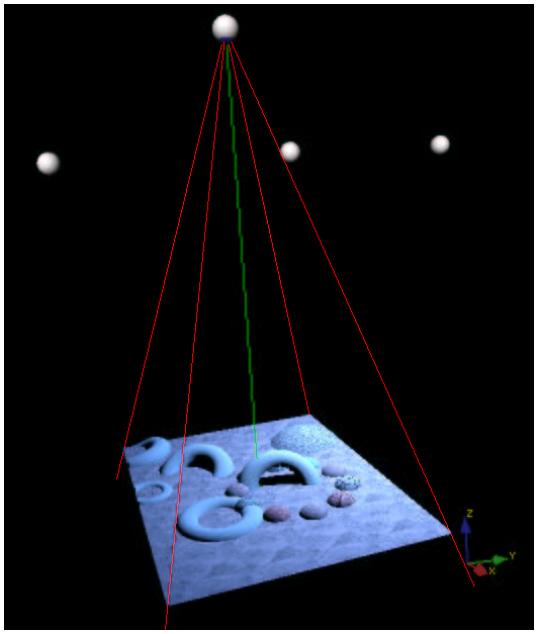

Fig. 2. Geometry of the system. The top sphere represents the position of the camera. The part of the scene viewed by the camera is illustrated through the red lines. The other 3 spheres represent the position of the light sources

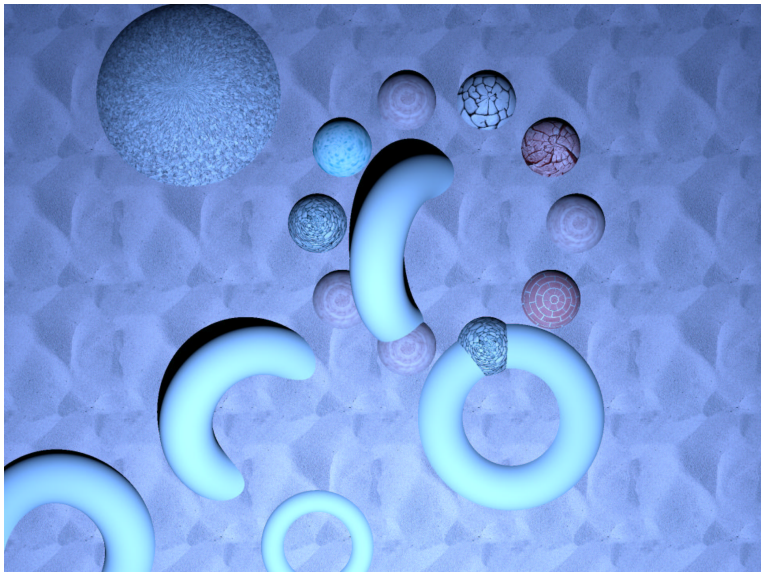

(a)

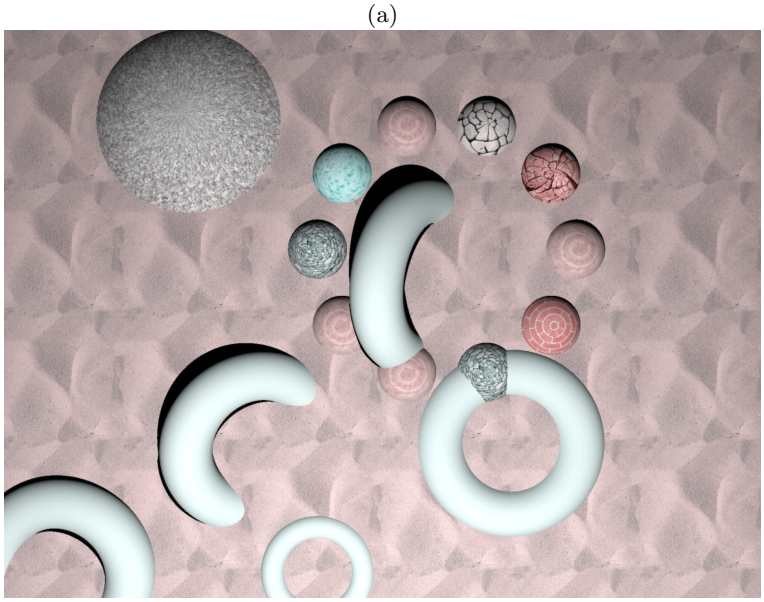

(b)

Fig. 3. (a) Original synthetic image. (b) Reconstructed image after removing the absorption effect (continuous case)

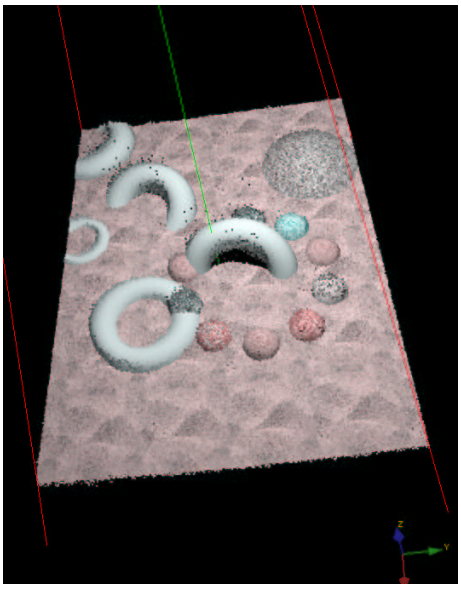

Fig. 4. Resulting 3D geometric and reflectance reconstruction after adding realistic noise to the acquired image, absorption parameters, power of the lamps and the system geometry

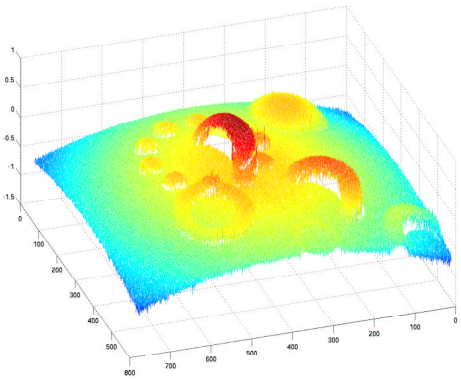

Fig. 5. Depth-map (d) of the reconstructed scene obtained from the noisy input data. The reference coordinate system is located at the focal point of the camera